Observation of the Disorder-Induced Crystal-to-Glass Transition

Peter Yunker,[1] Zexin Zhang,[1,2] and A. G. Yodh[1]

[1]Department of Physics and Astronomy, University of Pennsylvania, Philadelphia, Pennsylvania 19104, USA
[2]Complex Assemblies of Soft Matter, CNRS-Rhodia-UPenn UMI 3254, Bristol Pennsylvania 19007, USA

(Received 30 October 2009; revised manuscript received 9 December 2009; published 8 January 2010)

The role of frustration and quenched disorder in driving the transformation of a crystal into a glass is investigated in quasi-two-dimensional binary colloidal suspensions. Frustration is induced by added smaller particles. The crystal-glass transition is measured to differ from the liquid-glass transition in quantitative and qualitative ways. The crystal-glass transition bears structural signatures similar to those of the crystal-fluid transition: at the transition point, the persistence of orientational order decreases sharply from quasilong range to short range, and the orientational order susceptibility exhibits a maximum. The crystal-glass transition also features a sharp variation in particle dynamics: at the transition point, dynamic heterogeneity grows rapidly, and a dynamic correlation length scale increases abruptly.

DOI: 10.1103/PhysRevLett.104.015701 PACS numbers: 64.70.kj, 61.43.Fs, 64.70.pv, 82.70.Dd

Disorder plays a critical role in traditional melting and freezing phenomena and in the formation of glasses. Melting from crystal to fluid, for example, is a sharp transition accompanied by loss of orientational and translational order and by a dramatic decrease in flow resistance and rearrangement time scale [1]. By contrast, orientational and translational order do not change significantly at the liquid-to-glass transition, even as viscosity and rearrangement time scale diverge [2]; nevertheless, frozen-in residual disorder is critical for glass formation. An interesting, less-studied but closely related problem [3–6] concerns the role played by frustration and disorder in driving the transformation of a crystal to a glass. Herein we describe experiments which explore this transition, from crystalline solid to glass as a function of quenched disorder. The resultant glassy phases acquire typical properties such as dynamic heterogeneity [6–9] and disorder, but the crystal-to-glass transition is quite sharp, exhibiting features often associated with melting.

Investigations of glass transitions and structural arrest are of broad interest, in part because the new concepts thus generated affect understanding of a wide variety of materials across a wide swath of scientific communities [6,8–12], including molecular [13], colloidal [9], granular [14], and polymeric [15] glasses. The experiments reported in this contribution relate closely to studies exploring how polydispersity prevents crystallization [16]. Our investigation, however, differs from the above in important ways; single-particle spatial resolution, for example, permits quantitative exploration of orientational order and dynamic heterogeneity as a function of packing fraction and disorder across the crystal-glass transition.

The experiments employ temperature-dependent nearly hard-sphere binary colloidal suspensions composed of two particle sizes with substantially different diameters [12,17]. The number fraction of the smaller diameter ''dopant'' particles is varied from 0.0 to 0.5, and the area fraction of the two-dimensional (2D) suspension is varied from $\sim$0.75 to $\sim$0.90 at each dopant concentration. This approach enables us to trace sample evolution as function of increasing quenched disorder at fixed area fraction. Structural correlations associated with orientational order and dynamic correlations associated with particle rearrangements are measured. The path from crystal to glass is marked by a sharp drop in structural correlations and a sudden jump in dynamical correlations. The crystal-glass transition bears structural signatures similar to the crystal-fluid transition [1,18]: the orientational order correlation function changes form abruptly from quasilong range to short range at the transition point, and the orientational order susceptibility exhibits a maximum at the transition point. A similarly sharp transition from homogeneous to heterogeneous dynamics accompanies these structural changes; in particular, domains of correlated particle rearrangements (i.e., dynamic heterogeneity) appear to turn on suddenly, and a dynamic correlation length scale increases sharply from $\sim$2 to $\sim$6 particle diameters across the transition point. The crystal-to-glass transition is thus measured to differ from the liquid-to-glass transition in qualitative and quantitative ways.

Binary mixtures of repulsive particles have been used as model glasses in experiment [12,17,19] and simulation [10,20,21]. The present experiment employs aqueous suspensions of micron-size poly(*N*-isopropyl acrylamide) microgel colloidal spheres (i.e., NIPA particles), whose diameters increase as temperature is reduced [22]. The particles are very similar to those used in recent phase transformation experiments and are described therein [12,17,18,23]. A binary mixture of NIPA particles is sandwiched between two glass cover slips, creating a quasi-2D system. The sample consists of a mixture of NIPA spheres with small and large diameters, $D_S = 1.09\ \mu$m and $D_L = 1.55\ \mu$m, respectively, at temperature $T = 28.0\,^{\circ}$C. The polydispersity of each particle type is $\sim$3%, and the par-

ticle interaction potentials are short-range repulsive with a soft tail [18].

We synthesized many bidisperse suspensions with varying small particle number fractions, n_S (i.e., $n_S = 0.00, 0.01, 0.02, 0.04, 0.05, 0.07, 0.10, 0.15, 0.20, 0.28, 0.50$). By adjusting the sample temperature using a microscope objective heater (BiOptechs), the area fraction ϕ_A was readily increased from $\phi_A \approx 0.75$ to $\phi_A \approx 0.90$ with a step size of ~ 0.01 in ϕ_A. Figure 1 summarizes n_S and ϕ_A in every sample. Trajectories with varying n_S and fixed ϕ_A can be constructed by following a horizontal line across the diagram. Data were collected at each ϕ_A/n_S combination for 3000 s at a video rate of 3 frames per second. The field of view was 60 μm by 80 μm and contained ~ 2000 particles.

Orientational order is characterized by the bond orientational order parameter: $\psi_6 = \frac{1}{N_{\mathrm{tot}}\mathrm{CN}} \sum_{j=1}^{N_{\mathrm{tot}}} \sum_{k=1}^{\mathrm{CN}} |e^{i6\theta_{jk}}|$, where θ_{jk} is the angle between the x axis and the $j-k$ bond between particles j and k, CN is the coordination number of particle j, and N_{tot} is the total number of particles. The value of ψ_6 at $\phi_A = 0.85$ is plotted as a function of n_S in Fig. 2(b). As n_S increases from 0, ψ_6 decays as a power law. Additionally, the areal density of free disclinations N_D was measured to increase sharply and then stabilize for larger n_S [Fig. 2(c)]. Breakup of dislocations (free and bound) into free disclinations is typically associated with formation of the liquid phase [1,18].

To characterize the spatial persistence of orientational order, the correlation function $g_6(r = |\mathbf{r}_i\text{-}\mathbf{r}_j|) = \langle \psi_{6i}^*(r_i)\psi_{6j}(r_j)\rangle$, where r_i and r_j are the positions of particles i and j, is derived from the data [Fig. 2(d)]. Two distinct regimes corresponding to crystal and glass are quantitatively identified: $g_6 \sim r^{-\eta}$ (quasilong range) for the crystalline state ($n_S < 0.02$) and $g_6 \sim e^{-r/\xi_6}$ (short range) for the glass state ($n_S \geq 0.02$). By contrast, g_6 changes very little across the liquid-to-glass transition [2].

Temporal fluctuations in ψ_6 are characterized by the susceptibility: $\chi_6 = N_{\mathrm{tot}}(\langle(\bar{\psi}_6)^2\rangle - \langle\bar{\psi}_6\rangle^2)$, where $\bar{\psi}_6$ is the average of ψ_6 within one image frame ($\bar{\psi}_6 = \sum_{i=1}^{N_{\mathrm{tot}}} |\psi_6|/N_{\mathrm{tot}}$), and angle brackets indicate average over time [see Fig. 2(a)]. To ameliorate finite-size effects, χ_6 is calculated in multiple sub-boxes containing different numbers of particles and is then extrapolated to the infinite size limit [18] (see supplemental material [24]). Interestingly, this susceptibility reaches its maximum at $n_S = 0.02$, the same value of n_S that marks the change from quasilong-range orientational order to short-range orientational order [i.e., the dashed line in Figs. 2(a)–2(c)]. Thus the variation of both the correlation length and the orientational order susceptibility, χ_6, suggests a sharp transition between crystal (ordered) and glass (disordered) states as a function of quenched disorder.

The sharp decrease in orientational order correlation length, the peak in χ_6 (ψ_6 susceptibility), and the increase in defects (free disclinations) associated with the liquid state are all reminiscent of the crystal-liquid transition [1,18], suggesting a distinct transition from crystal to glass via increasing quenched disorder [5]. This result stands in contrast to the transition from liquid to glass, where

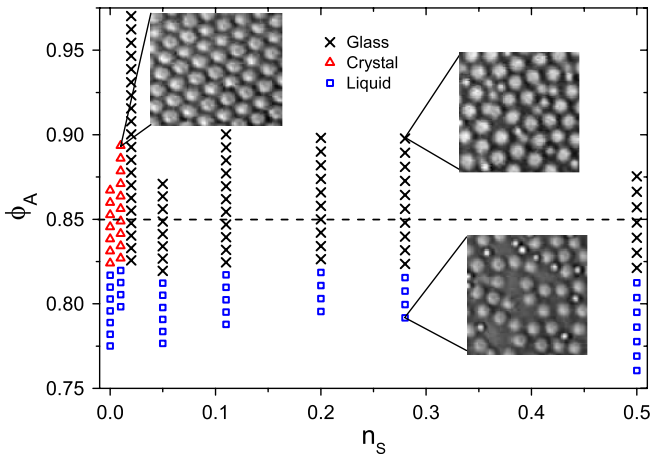

FIG. 1 (color online). Diagram summarizing all collected data. The crystalline phase is plotted with triangles, the glass phase is plotted with crosses, and the liquid phase is plotted with squares. Data presented in the remainder of the Letter come from points touching the dashed line. Experimental microscope images of sample subregions are displayed from suspensions with $n_S = 0.01$, $\phi_A = 0.89$ (crystal), $n_S = 0.28$, $\phi_A = 0.90$ (glass), and $n_S = 0.28$, $\phi_A = 0.79$ (liquid).

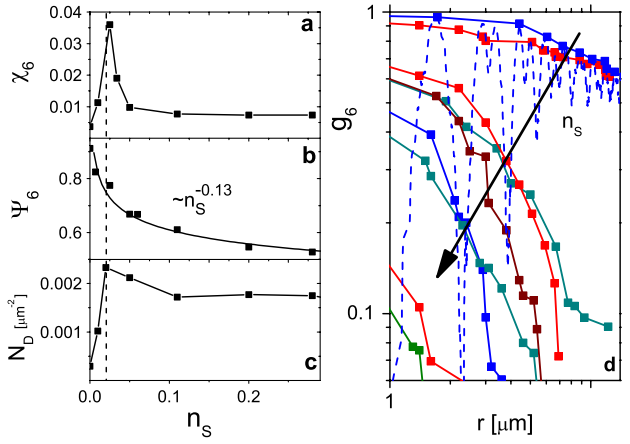

FIG. 2 (color online). (a) The bond orientational order parameter (ψ_6) susceptibility, χ_6, versus n_S, at area fraction $\phi_A = 0.85$. The dashed line marks $n_S = 0.02$, the point where χ_6 reaches its maximum value. The solid line guides the eye. (b) ψ_6 versus n_S, at area fraction $\phi_A = 0.85$. The solid line is a power law fit. (c) Free disclination density N_D, the number disclinations per μm^2, versus n_S at $\phi_A = 0.85$. The solid line guides the eye. (d) Envelope of the local maxima of the orientational order spatial correlation functions $g_6(r)$ for $n_S = 0.00, 0.01, 0.02, 0.05, 0.11, 0.20, 0.28, 0.50$, and packing fraction $\phi_A = 0.85$. The complete (oscillating) g_6 is shown for $n_S = 0.01$ (dashed line).

changes in structural correlations are not observed [2]. Thus the present system appears to be an excellent new model for study of the relationship between structural order and glass dynamics (e.g., dynamic heterogeneity).

To explore dynamical variations with n_S, we first compute the two-point self-correlation function: $Q_2(d_L, \Delta t) = \frac{1}{N_{\rm tot}} \sum_{i=1}^{N_{\rm tot}} \exp(-\Delta r_i^2/2d_L^2)$ [25]. Here d_L is a preselected length scale to be probed and Δr_i is the distance particle i moves in time Δt. If a particle moves a distance smaller than d_L, Q_2 will be close to 1; if a particle moves a distance greater than d_L, Q_2 will be close to 0. Plots of Q_2 for $d_L = 0.05$ μm are given in Fig. 3(a). For the crystalline states ($n_S < 0.02$), Q_2 plateaus and does not decay within the experimental window. Conversely, for glass states, Q_2 decays within the observed time frame, due to the rearrangement of particle cages as the particles seek new configurations. This effect was first noted in [4].

The emergence of domains of correlated rearrangements is central to many different properties of glasses [6–9]. This so-called dynamic heterogeneity is characterized by temporal fluctuations in Q_2, and these fluctuations are commonly quantified by the dynamic susceptibility [8,25,26], $\chi_4(d_L, \Delta t) = N_{\rm tot}(\langle Q_2(d_L, \Delta t)^2\rangle - \langle Q_2(d_L, \Delta t)\rangle^2)$, as a function of length scale d_L and time scale Δt. The variation of χ_4 with n_S, at the value of d_L that maximizes the peak in χ_4, is plotted in Fig. 3(b) for $\phi_A = 0.85$ and $n_S = 0.0$, 0.01, 0.025, 0.07, and 0.16. For $n_S > 0.02$, χ_4 exhibits a peak similar to that found in previous works [8,25–28]. Conversely, χ_4 is small and flat for samples with $n_S < 0.02$, as expected for crystalline systems.

The maximum value of χ_4 (i.e., χ_4^*) is plotted in Fig. 4(a) for each n_S at $\phi_A = 0.85$. In crystalline suspensions, χ_4^* is small ($\sim$1). Once n_S is increased beyond 0.02, however, χ_4^* jumps discontinuously to $\sim$35. As n_S is increased still further, χ_4^* remains fairly constant. This sharp change is absent in the liquid-glass transition [8,28]. For comparison we plot χ_4^* across the liquid-glass transition in this same experimental system as a function of particle area fraction at fixed dopant concentration $n_S = 0.25$ (i.e., along the vertical line with $n_S = 0.25$ in Fig. 1); χ_4^* increases continuously as packing fraction is increased [Fig. 4(b)], similar to [8,28].

χ_4^* can be related to the number of particles participating in a dynamically heterogeneous event [26]. The sudden variation of χ_4^* is thus indicative of a sudden increase in the size of domains of correlated rearranging particles as the system evolves from crystal to glass. When too much quenched disorder exists in the sample for crystallization to occur, the suspension is pushed out of equilibrium as it searches for a configuration to minimize its free energy. These search pathways are constrained by the suspension's large packing fraction, and rearrangements must occur in a collective manner. Interestingly, once in the glass phase, further increasing n_S moves χ_4^* to larger values of d_L [Fig. 4(c)], implying relaxation events are more effective. However, χ_4^* itself does not increase significantly, thus implying the degree of quenched order has little effect on the domain size of collective rearrangements (see supplemental material [24]).

To further characterize the domain size of the correlated rearrangements, we derived spatial correlations of $1 - Q_2^*$,

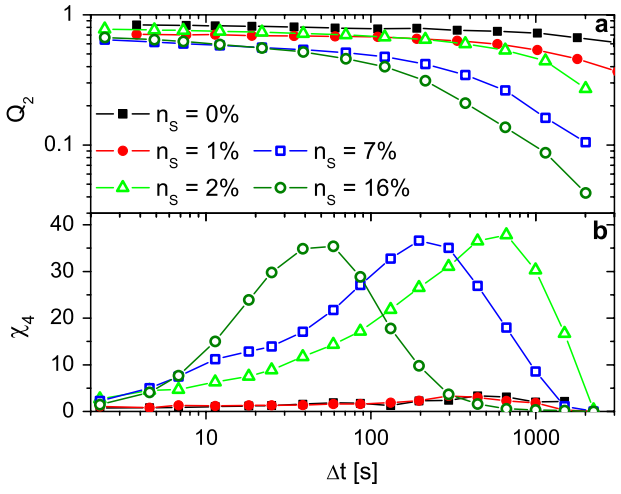

FIG. 3 (color online). (a) The two-point-correlation function Q_2 , is plotted versus Δt, for $d_L = 0.05$ μm and for $n_S = 0.00$ (solid squares), 0.01 (solid circles), 0.02 (open triangles), 0.07 (open squares), 0.16 (open circles). (b) The four-point dynamic susceptibility χ_4 is plotted versus Δ_t for the same values of n_S as in (a); the value of d_L is chosen to maximize peak height.

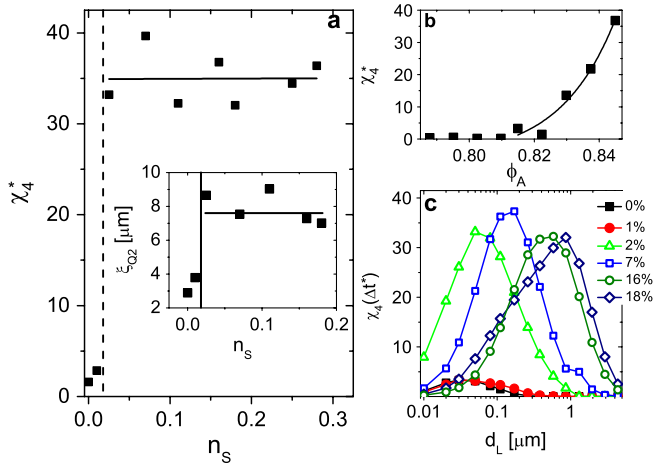

FIG. 4 (color online). (a) The maximum value of χ_4, χ_4^*, plotted versus the fraction of small particles n_S. The solid line is a linear fit, to guide the eye. The dashed line marks $n_S = 0.02$. Inset: Rearrangement correlation length ξ_{Q_2} versus n_S. The solid line is a linear fit to guide the eye. The dashed line marks $n_S = 0.02$. (b) χ_4^* plotted versus ϕ_A for $n_S = 0.25$. The solid line is a power law fit to guide the eye. (c) The maximum value of χ_4 is plotted as a function of d_L for four values of n_S.

yielding the rearrangement spatial correlation function: $g_{Q_2}(r = |\mathbf{r}_i\text{-}\mathbf{r}_j|) = \langle(1 - Q^*_{2i}(r_i))(1 - Q^*_{2j}(r_j))\rangle$. Here Q^*_2 is calculated for values of d_L and Δt that maximize χ_4, and thus dynamic heterogeneity. Note that correlations of $1 - Q^*_2$ relate to *rearranging* particles, i.e., particles moving farther than d_L. These correlation functions are readily fit by decaying exponentials ($g_{Q_2} \propto \exp(-r/\xi_{Q_2})$), and a correlation length ξ_{Q_2} is thus readily extracted [Fig. 4(a) inset). For crystalline samples ($n_S < 0.02$), $\xi_{Q_2} \sim 2D_L$, implying that when particles move large distances, only their nearest neighbors move large distances. For glass samples ($n_S > 0.02$), $\xi_{Q_2} \sim 6D_L$, implying that when particles move large distances, they do so in a correlated manner involving many particles. The size of ξ_{Q_2} jumps sharply at $n_S = 0.02$, along with the discontinuous increase in χ^*_4 (during the liquid-to-glass transition, ξ_{Q_2} follows the same continuous trend as χ^*_4). Thus the onset of dynamic heterogeneity appears nearly discontinuously.

The *dynamical* transition from crystal to glass is thus characterized by a discontinuous jump in χ^*_4, the maximum value of the dynamic susceptibility, and a discontinuous increase in spatial correlation decay length from $\sim 2D_L$ to $\sim 6D_L$. These results stand in contrast to the liquid-glass transition, during which dynamics change relatively more slowly and continuously. The rapid onset of glass dynamics occurs at the same value of n_S as the structural transition from crystal to glass. In other words, dynamic heterogeneity appears simultaneously with the disappearance of quasilong-range orientational order. To conclude, while the liquid-to-glass transition is somewhat ambiguous and often difficult to define, the crystal-to-glass transition with increasing quenched disorder appears sharp and unambiguously defined.

We thank Doug Durian, Piotr Habdas, Yilong Han, and Matt Lohr for useful discussions. We acknowledge the financial support of the National Science Foundation through DMR-080488 (A. G. Y.) and the PENN MRSEC DMR-0520020. Z. Z. gratefully acknowledges partial support from Rhodia.

[1] D. Nelson and B. Halperin, Phys. Rev. B **19**, 2457 (1979).
[2] A. van Blaaderen and P. Wiltzius, Science **270**, 1177 (1995).
[3] P. C. Royall, E. C. Vermolen, A. Blaaderen, and H. Tanaka, J. Phys. Condens. Matter **20**, 404225 (2008); S. I. Henderson, T. C. Mortensen, S. M. Underwood, and W. van Megen, Physica (Amsterdam) **233A**, 102 (1996); E. Zaccarelli *et al.*, Phys. Rev. Lett. **103**, 135704 (2009); G. Tarjus, S. Kivelson, Z. Nussinov, and P. Viot, J. Phys. Condens. Matter **17**, R1143 (2005); M. R. Sadr-Lahijany, P. Ray, and H. E. Stanley, Phys. Rev. Lett. **79**, 3206 (1997); S. Pronk and D. Frenkel, Phys. Rev. E **69**, 066123 (2004).
[4] T. Hamanaka and A. Onuki, Phys. Rev. E **75**, 041503 (2007).
[5] H. Fecht, Nature (London) **356**, 133 (1992); D. Nelson, Phys. Rev. B **27**, 2902 (1983).
[6] T. Kawasaki, T. Araki, and H. Tanaka, Phys. Rev. Lett. **99**, 215701 (2007); T. Kawasaki, T. Araki, and H. Tanaka, Phys. Rev. Lett. **100**, 099602 (2008).
[7] C. P. Royall, S. R. Williams, T. Ohtsuka, and H. Tanaka, Nature Mater. **7**, 556 (2008).
[8] L. Berthier *et al.*, Science **310**, 1797 (2005).
[9] E. Weeks, J. C. Crocker, A. C. Levitt, A. Schoeld, and D. Weitz, Science **287**, 627 (2000).
[10] C. O'Hern, S. Langer, A. Liu, and S. Nagel, Phys. Rev. Lett. **88**, 075507 (2002).
[11] A. Widmer-Cooper, H. Perry, P. Harrowell, and D. R. Reichman, Nature Phys. **4**, 711 (2008).
[12] Z. Zhang *et al.*, Nature (London) **459**, 230 (2009).
[13] H. W. Sheng, W. K. Luo, F. M. Alamgir, J. M. Bai, and E. Ma, Nature (London) **439**, 419 (2006).
[14] A. S. Keys, A. R. Abate, S. C. Glotzer, and D. J. Durian, Nature Phys. **3**, 260 (2007).
[15] I. M. Hodge, Science **267**, 1945 (1995).
[16] H. J. Schöpe, G. Bryant, and W. van Megen, J. Chem. Phys. **127**, 084505 (2007); S. Martin, G. Bryant, and W. van Megen, Phys. Rev. E **67**, 061405 (2003); D. A. Kofke and P. G. Bolhuis, Phys. Rev. E **59**, 618 (1999); S. Auer and D. Frenkel, Nature (London) **409**, 1020 (2001); S. Williams, I. Snook, and W. van Megen, Phys. Rev. E **64**, 021506 (2001); P. Bartlett and P. B. Warren, Phys. Rev. Lett. **82**, 1979 (1999); M. Fasolo and P. Sollich, Phys. Rev. Lett. **91**, 068301 (2003).
[17] P. Yunker, Z. Zhang, K. B. Aptowicz, and A. G. Yodh, Phys. Rev. Lett. **103**, 115701 (2009).
[18] Y. Han, N. Y. Ha, A. M. Alsayed, and A. G. Yodh, Phys. Rev. E **77**, 041406 (2008).
[19] L. Assoud, F. Ebert, P. Keim, R. Messina, G. Maret, and H. Löwen, Phys. Rev. Lett. **102**, 238301 (2009); J. M. Lynch, G. C. Cianci, and E. R. Weeks, Phys. Rev. E **78**, 031410 (2008).
[20] W. Kob, C. Donati, S. J. Plimpton, P. H. Poole, and S. C. Glotzer, Phys. Rev. Lett. **79**, 2827 (1997).
[21] V. Ilyin, I. Procaccia, I. Regev, and N. Schupper, Phys. Rev. E **77**, 061509 (2008).
[22] B. R. Saunders and B. Vincent, Adv. Colloid Interface Sci. **80**, 1 (1999); R. Pelton, Adv. Colloid Interface Sci. **85**, 1 (2000).
[23] A. M. Alsayed, M. Islam, J. Zhang, P. Collings, and A. G. Yodh, Science **309**, 1207 (2005); H. Senff and W. Richtering, J. Chem. Phys. **111**, 1705 (1999); J. Wu, B. Zhou, and Z. Hu, Phys. Rev. Lett. **90**, 048304 (2003); Y. Han *et al.*, Nature (London) **456**, 898 (2008).
[24] See supplementary material at http://link.aps.org/supplemental/10.1103/PhysRevLett.104.015701 for more details about dynamics and data analysis.
[25] R. Candelier, O. Dauchot, and G. Biroli, Phys. Rev. Lett. **102**, 088001 (2009).
[26] A. R. Abate and D. J. Durian, Phys. Rev. E **76**, 021306 (2007).
[27] S. Glotzer, J. Non-Cryst. Solids **274**, 342 (2000).
[28] A. R. Abate and D. J. Durian, Phys. Rev. Lett. **101**, 245701 (2008).